J. Fluid Mech. (2002), *vol.* 473, *pp.* 295–319.
DOI: 10.1017/S0022112002002422 Printed in the United Kingdom

Energy propagation of long extratropical Rossby waves over slowly varying zonal topography

By RÉMI TAILLEUX[1] AND JAMES C. McWILLIAMS[2]

[1]Laboratoire de Météorologie Dynamique, UPMC Paris 6, Case courrier 99, 4 Place Jussieu, 75252 Paris Cédex 05, France

[2]Institute of Geophysics and Planetary Physics, UCLA, CA 90095-1567, USA

(Received 6 November 2001 and in revised form 24 July 2002)

In classical WKB theory the only way wave energy density, as a surrogate for wave action density, can increase or decrease along a ray is as a result of the ray focusing or widening. This occurs when the group velocity is divergent. There are particular regions, however, where the wave can resonantly exchange action with another wave mode with approximately the same wavenumbers; a situation known as Landau–Zener transition, mode conversion, linear (adiabatic) resonance, etc. This effect invalidates locally the underlying assumption of WKB theory that no scattering of energy occurs between WKB wave modes. In this paper this effect is investigated theoretically for free long baroclinic Rossby waves in a two-layer planetary geostrophic model of the ocean with a purely zonal topography, here taken as a Gaussian ridge. The waves are excited along the east coast by an unspecified wavemaker at a fixed frequency ω. In the computation considered, mode conversion is found to occur principally near the ridge's top and on the eastern flank. The predictions of mode conversion theory are tested against the results of direct numerical simulations. This shows excellent agreement, both for the locations of mode conversion points, and for the amplitude of the transmitted and converted WKB wave modes.

1. Introduction

Recently, the effects of a realistic varying environment on the propagation of baroclinic Rossby waves in the ocean have received increased attention, motivated by the TOPEX/Poseidon altimeter data analysis by Chelton & Schlax (1996) showing: (i) evidence that first-mode baroclinic Rossby waves propagate faster at mid- and high-latitudes than expected from the linear standard normal modes theory (Leblond & Mysak 1978; Gill 1982); and (ii) a marked increase of baroclinic wave activity westward of major topographic features suggesting a topographic role in creating/amplifying incident baroclinic Rossby waves. In order to account for these effects, most recent theoretical investigations have focused on the influence of the background mean flow and topography, which are both ignored in the linear standard theory. Assuming a scale separation between the 'varying environment' and the waves, a reasonable first step, the issue can be addressed by means of WKB theory.

Within that framework, the first issue, i.e. the anomalous propagation of Rossby waves, can be addressed by solving a modified eigenvalue problem. This is the approach pursued by most studies so far, the majority focusing on only the mean flow effect, (e.g. Killworth, Chelton & deSzoeke 1997; Dewar 1998; Liu 1999); the effects of topography were discussed by Killworth & Blundell (1999, hereinafter

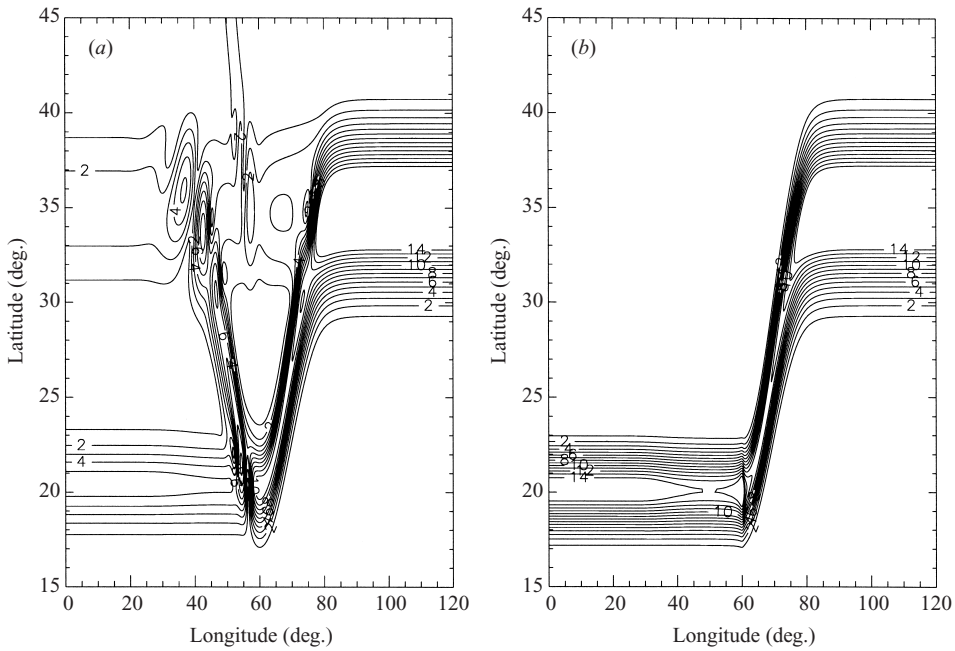

FIGURE 1. The root-mean square of the interface displacement as computed by (*a*) direct numerical simulation, and (*b*) from the wave action ray tube conservation equation of single mode WKB theory. Note that the contour lines represent isolines, not rays.

referred to as KB99) and Tailleux & McWilliams (2000, hereinafter referred to as TM00). Since this issue is beyond the scope of this paper, the interested reader is referred to Tailleux & McWilliams (2001) for further references and discussion. The latter paper also provides a discussion of the impact of the bottom boundary condition on the solution of the eigenvalue problem.

Addressing issue (ii) – related to the increase of wave activity westward of major topographic features – poses interesting questions within the framework of WKB theory that constitute the motivation for this paper. Indeed, in classical WKB theory, the only way energy – here taken as a surrogate for the more general concept of action – can increase or decrease along a ray is as a result of the ray focusing or widening, which occurs when the group velocity is divergent. In this view, action is conserved along a ray without exchange with rays of a different nature, i.e. representing other allowable wave modes. On this basis, KB99 invoked ray focusing to account for the observed increase of baroclinic wave activity westward of major topographic features. However, on the basis of direct numerical computations, TM00 found that an initial purely baroclinic mode systematically transferred part of its energy to the barotropic mode over a ridge surrounded by flat-bottom regions on its western and eastern parts. Starting with only one mode in the eastern flat-bottom part, two modes were systematically found in the western flat-bottom part. TM00 concluded that the assumption of no energy scattering between modes, made by KB99 in a continuously stratified fluid, was not valid in their two-layer model. The failure of single-mode WKB theory in that case is demonstrated in figure 1 which compares a direct numerical computation (figure 1*a*) with the solution predicted by single-mode WKB theory (figure 1*b*) for an 'eastern wavemaker experiment' similar to that used previously in KB99 and TM00 and described in more detail later in the text. The geometry of the

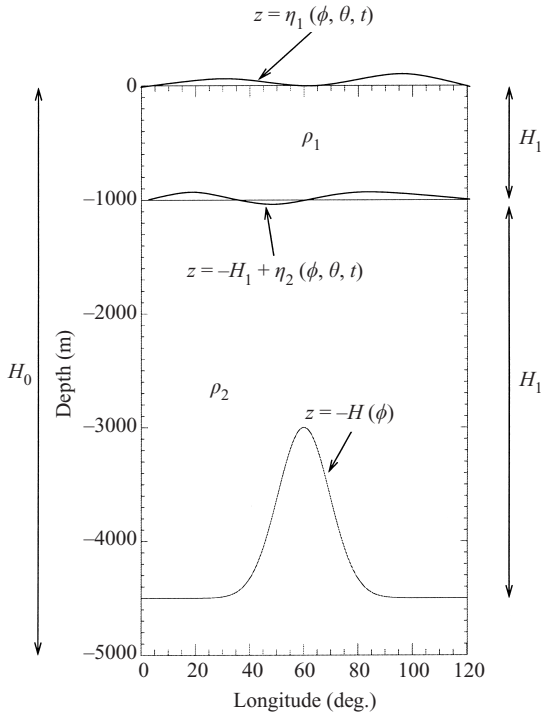

FIGURE 2. Model geometry and notation.

two-layer model is depicted schematically in figure 2. Figure 1 makes it clear that the energy does not stay with a single ray, but that it successively splits as it propagates westward. In that case, a first separation appears to occur at the bottom of the ridge, whereas a second separation, more pronounced, is visible near the top of the ridge.

The purpose of this work is to gain insight into the coupling of the WKB modes, because this appears to be necessary to provide a complete descriptor of the energy propagation of baroclinic Rossby waves in a varying environment, here limited for simplicity to a purely zonally varying topography without a background mean flow. In the early stages of this work, it was at first unclear how to interpret this issue within the framework of WKB theory because the coupling of the WKB modes is intrinsically associated with a case of WKB breakdown unrelated to caustics (the latter being well understood). In contrast, it was easy to interpret this coupling in terms of JEBAR (joint effect of baroclinicity and relief), which is somehow the natural 'reflex' in oceanography, e.g. Sakamoto & Yamagata (1997). The invocation of JEBAR merely amounts to saying that the standard modes are coupled everywhere over topography, which is somewhat obvious given that they are no longer dynamical modes. Theoretically, it is also very difficult to quantify precisely the energy transfer between the standard modes over topography (TM00). A different approach was followed by Hallberg (1997, hereinafter referred to as H97) who suggested, based on comparisons between ray calculations and direct numerical simulations, that the coupling of WKB modes be regarded as localized and thus pointwise in nature. In the coupling region, H97 speaks of an 'incident' ray splitting into a 'reflected' and a 'transmitted' ray, drawing an analogy with classical wave reflection theory. Arguing that mass conservation locally strongly constrains the solution, H97 also derived empirical arguments to quantify the transmitted and reflected wave energy.

Although little studied in oceanography, the topic of WKB mode coupling has been nevertheless extensively studied in other fields, most notably in plasma physics where the phenomenon is dealt with by so-called mode conversion theory (e.g. Kaufman & Friedland 1987; Flynn & Littlejohn 1994). Physically, mode conversion appears as a particular case of linear resonance occurring when the frequency and wavenumbers of two distinct wave modes locally satisfy approximately the same dispersion relation. In other words, mode conversion occurs at points where two different branches of a given dispersion relation osculate. In an oceanographic context, the main ingredients of the theory were derived independently by Grimshaw & Allen (1979) to understand a case of mode conversion involving Kelvin and coastal-trapped waves investigated by Allen & Romea (1980), but the study stopped short of quantifying the possible transmission between branches. Recently, Kaufman *et al.* (1999) made a technology transfer from plasma physics to oceanography in order to address the mode conversion of coastal Kelvin and Yanai waves in the Gulf of Guinea. Vanneste (2001, hereinafter referred to as V01) discussed the relevance of mode conversion theory to account for the results of H97, yet did not test the theory in the particular settings considered by Hallberg. Instead, he simply showed how to apply the theory to the particular case of a purely meridional topography that is the most tractable, but arguably less relevant for H97's study, while questioning the validity of Hallberg's mass conservation arguments suggesting widespread coupling. In reply, Hallberg (2001, hereinafter referred to as H01) maintained the previous claims of widespread coupling. By using mode conversion theory to compute the transmission coefficient for a purely zonal topography in the long-wave limit, he furthermore argued that mode conversion theory did not contradict the previous estimates based on mass conservation arguments.

Even though undoubtedly relevant to the issue of linear WKB mode coupling, none of these studies offers a direct comparison between the predictions of mode conversion theory and an exact solution. Furthermore, these studies are only concerned with the strength of the linear coupling, although another interesting prediction of mode conversion theory concerns the physical location of the linear coupling. In this paper, we go beyond the studies by H97, V01 and H01 by offering a detailed analysis of mode conversion theory by comparing its predictions directly with an 'exact' solution computed numerically. In addition, attention is paid to simplifying the ray equations, in order to obtain a semi-analytical description of all WKB quantities. Similarly to H01, we consider the case of a purely zonal topography, but planetary geostrophy is used in place of quasi-geostrophy. This allows for the propagation of Rossby waves to vary with latitude.

The manuscript is organized as follows. The model features are introduced in § 2. The WKB analysis is presented in § 3. This section analyses and greatly simplifies the ray and action conservation equations. Section 4 focuses on the qualitative and quantitative aspects of mode conversion for the present model. The results are discussed and conclusions are drawn in § 5.

2. Model features

2.1. *The model*

We use a two-layer model of the ocean circulation – as we did in TM00. Furthermore, we use the planetary geostrophic approximation since we are interested only in large-scale disturbances on time scales much longer than a pendulum day. The model

geometry and notation are summarized in figure 2. Specifically, H_1 and $H_2 = H(\phi) - H_1$ represent the unperturbed layer thicknesses, respectively, with $H(\phi)$ the total ocean depth assumed here to be a function of longitude only; $\eta_1(\phi, \theta, t)$ and $\eta_2(\phi, \theta, t)$ represent the perturbed surface and interface displacements, with θ the latitude and t the time; the total layer thicknesses are thus $h_1 = H_1 + \eta_1 - \eta_2$ and $h_2 = H_2 + \eta_2$; ρ_1 and ρ_2 are the densities of the homogeneous inviscid upper and lower layers, respectively; $\epsilon = (\rho_2 - \rho_1)/\rho_0$ is a dimensionless measure of the density difference across the layer interface; $\boldsymbol{U}_i = h_i \boldsymbol{u}_i \approx H_i \boldsymbol{u}_i$ is the (linearized) horizontal transport in layer $i = 1, 2$; p_i is the horizontal part of the hydrostatic pressure divided by the reference density ρ_0 involved in the Boussinesq approximation; $f = 2\Omega \sin\theta$ is the Coriolis parameter, where Ω is the Earth's rotation rate; R is the Earth's radius; g is the Earth's acceleration due to gravity, and $g' = g\epsilon$. The planetary geostrophy equations thus read

$$f\hat{\boldsymbol{z}} \times \boldsymbol{U}_i + H_i \nabla p_i = 0 \qquad (i = 1, 2), \tag{2.1}$$

$$\frac{\partial(\eta_1 - \eta_2)}{\partial t} + \mathrm{div}\boldsymbol{U}_1 = 0, \tag{2.2}$$

$$\frac{\partial \eta_2}{\partial t} + \mathrm{div}\boldsymbol{U}_2 = 0. \tag{2.3}$$

Equation (2.1) is the classical geostrophic approximation, whereas (2.2) and (2.3) express mass conservation in each layer. For hydrostatic motions, p_1 and p_2 are related to the surface and interface displacements by $p_1 = g\eta_1$ and $p_2 = g(\eta_1 + \epsilon\eta_2)$. By combining (2.1) with (2.2) and (2.3), a system of equations for only the pressure perturbations can be derived; it can be written concisely as follows:

$$\boldsymbol{S}\frac{\partial \boldsymbol{p}}{\partial t} + \frac{g'}{R^2 \cos\theta}\left[\boldsymbol{D}_\phi \frac{\partial \boldsymbol{p}}{\partial \phi} + \boldsymbol{D}_\theta \frac{\partial \boldsymbol{p}}{\partial \theta}\right] = 0, \tag{2.4}$$

where $\boldsymbol{S}$, $\boldsymbol{D}_\phi$ and $\boldsymbol{D}_\theta$ are the following symmetric matrices:

$$\boldsymbol{S} = \begin{pmatrix} 1+\epsilon & -1 \\ -1 & 1 \end{pmatrix}, \tag{2.5}$$

$$\boldsymbol{D}_\phi = \begin{pmatrix} \mathscr{U}_1^\phi & 0 \\ 0 & \mathscr{U}_2^\phi \end{pmatrix}, \quad \boldsymbol{D}_\theta = \begin{pmatrix} \mathscr{U}_1^\theta & 0 \\ 0 & \mathscr{U}_2^\theta \end{pmatrix}, \tag{2.6}$$

with $\boldsymbol{p} = (p_1, p_2)^T$, the vector for the pressure perturbations. For the reader unfamiliar with the planetary geostrophy equations, note that (2.4) can also be obtained from the more widely known two-layer quasi-geostrophy equations, used for instance in Hallberg (1997), by (i) taking the long-wave limit, obtained by neglecting the Laplacian terms, (ii) retaining the latitudinal variations of f and β, (iii) by replacing the streamfunctions Ψ_i by the pressure perturbations p_i, and (iv) by rewriting everything in spherical-polar coordinates. The vectors $\mathscr{U}_i$ are related to the potential vorticity field H_i/f associated with the layer i by

$$\mathscr{U}_i^\phi = \frac{\partial}{\partial\theta}\left(\frac{H_i}{f}\right), \quad \mathscr{U}_i^\theta = -\frac{\partial}{\partial\phi}\left(\frac{H_i}{f}\right). \tag{2.7}$$

It follows that the matrices $\boldsymbol{D}_\phi$ and $\boldsymbol{D}_\theta$ satisfy the property $\partial_\phi \boldsymbol{D}_\phi + \partial_\theta \boldsymbol{D}_\theta = 0$. In the following, the problem is further simplified by making the rigid-lid approximation

that consists of taking the limit $\epsilon \longrightarrow 0$ for the matrix $\boldsymbol{S}$ in (2.5). The consequence of the rigid-lid approximation is to render $\boldsymbol{S}$ singular which is then no longer positive definite. It has a null-space generated by $\mathscr{W} = (1,1)^T$, the standard barotropic mode.

2.2. *Eastern wavemaker experiment*

In this paper, baroclinic Rossby waves are assumed to originate from the eastern boundary, where an unspecified wavemaker excites them at the annual period. Such a procedure is useful to study the propagation of free Rossby waves and was previously used in KB99 and TM00. Furthermore, we assume that the wavemaker excites waves only in the finite interval $[\theta_{min}, \theta_{max}]$. Denoting the middle of the latter interval by θ_{mid}, the interface displacement is specified at the eastern boundary at all times by

$$\eta_2(\phi_E, \theta, t) = \eta_0 \left(1 + \cos\left(2\pi \frac{\theta - \theta_{mid}}{\theta_{max} - \theta_{min}}\right)\right)^2 \mathrm{e}^{\mathrm{i}\omega t} + \text{c.c.} \quad (\theta_{min} \leqslant \theta \leqslant \theta_{max}).$$

We verify that both η_2 and $\mathrm{d}\eta_2/\mathrm{d}\theta$ vanish at θ_{min} and θ_{max} so that η_2 goes smoothly toward zero at the bounds of the interval. The zonally varying topography is taken as a Gaussian ridge,

$$H(\phi) = H_0 - \delta H \exp\left\{-\frac{1}{2}\left(\frac{\phi - \phi_0}{\delta\phi}\right)^2\right\}, \tag{2.8}$$

whereas the ocean basin is assumed to be bounded in longitude between the two meridians $\phi = 0$ and $\phi = \phi_E$. In latitude, we assume only that we are sufficiently far away from the equator for geostrophy to remain valid and that $f > 0$ corresponding to the northern hemisphere. The numerical experiment that constitutes the main illustration of this paper uses the following specific values: $H_1 = 1000\,\mathrm{m}$, $H_0 = 4500\,\mathrm{m}$, $\delta H = 1500\,\mathrm{m}$, $g' = 2 \times 10^{-2}\,\mathrm{ms}^{-2}$, $\omega = 2\pi/(1\,\text{year})$, $\delta\phi = 9.6^\circ$, $\theta_{max} - \theta_{min} = 26.33^\circ$, $\theta_{mid} = 35^\circ$, $\phi_0 = 60^\circ$, $\phi_E = 120^\circ$ and $\eta_0 = 5\,\mathrm{m}$.

2.3. *Remark on using spherical-polar coordinates*

Using spherical-polar coordinates for WKB theory requires attention to the scale factors which introduce some differences with the familiar form of the equations usually given in Cartesian coordinates. To that end, it is useful to introduce the notation,

$$\mathscr{U}_i^\star = \frac{g'}{R^2 \cos\theta} \mathscr{U}_i, \tag{2.9}$$

and $(\boldsymbol{D}_\phi^\star, \boldsymbol{D}_\theta^\star) = g'(\boldsymbol{D}_\phi, \boldsymbol{D}_\theta)/(R^2 \cos\theta)$. This allows us to rewrite (2.4) as follows:

$$\boldsymbol{S}\frac{\partial p}{\partial t} + \boldsymbol{D}_\phi^\star \frac{\partial p}{\partial \phi} + \boldsymbol{D}_\theta^\star \frac{\partial p}{\partial \theta} = 0, \tag{2.10}$$

which will prove more convenient for the WKB analysis. Furthermore, the transformation matrix

$$\mathscr{C} = \frac{1}{R}\begin{pmatrix} 1 & 0 \\ 0 & 1/\cos\theta \end{pmatrix}, \tag{2.11}$$

allows $\mathscr{U}_i$ to be written in terms of the coordinate-independent notation $\mathscr{C}\mathscr{U}_i =$

$-\hat{\boldsymbol{z}} \times \boldsymbol{\nabla}(H_i/f)$ so that $\mathrm{div}(\mathscr{C}\boldsymbol{\mathcal{U}}_i) = 0$ for $i = 1, 2$. As a consequence,

$$\frac{1}{R^2 \cos\theta}\left[\frac{\partial(\mathscr{A}\mathcal{U}_i^{\phi})}{\partial\phi} + \frac{\partial(\mathscr{A}\mathcal{U}_i^{\theta})}{\partial\theta}\right] = \mathrm{div}(\mathscr{A}\mathscr{C}\boldsymbol{\mathcal{U}}_i), \tag{2.12}$$

for any arbitrary scalar quantity $\mathscr{A}$.

2.4. *Energetics*

A conservation equation for the energy is obtained by multiplying the left-hand side of (2.4) by p^T; it can be written as

$$\frac{\partial \mathscr{E}}{\partial t} + \mathrm{div}\boldsymbol{\mathscr{F}} = 0, \tag{2.13}$$

with

$$\mathscr{E} = \tfrac{1}{2} p^T \boldsymbol{S} p = \tfrac{1}{2}[(p_2 - p_1)^2 + \epsilon p_1^2] = \tfrac{1}{2}[g'^2\eta_2^2 + \epsilon g^2 \eta_1^2], \tag{2.14}$$

$$\boldsymbol{\mathscr{F}} = \tfrac{1}{2} g'[p_1^2 \mathscr{C}\boldsymbol{\mathcal{U}}_1 + p_2^2 \mathscr{C}\boldsymbol{\mathcal{U}}_2]. \tag{2.15}$$

The energy (2.14) is the available potential energy of the system for planetary geostrophic motions. This energy reduces to $\mathscr{E} = \frac{1}{2} g'^2 \eta_2^2$ when the rigid-lid approximation made here is used, as this amounts to setting ϵ to zero in (2.14). For purely time periodic solution $(p_1, p_2) = (\hat{p}_1(\phi, \theta), \hat{p}_2(\phi, \theta))\, \mathrm{e}^{-\mathrm{i}\omega t}$, it is possible to show that the energy equation yields

$$\mathrm{div}(|\hat{p}_1|^2 \mathscr{C}\boldsymbol{\mathcal{U}}_1 + |\hat{p}_2|^2 \mathscr{C}_2 \boldsymbol{\mathcal{U}}_2) = 0, \tag{2.16}$$

where $|\hat{p}_i| = (\hat{p}_i \hat{p}_i^*)^{1/2}$ is the modulus of $\hat{p}_i$, the asterisk denoting complex conjugation.

3. WKB analysis and solution

3.1. *Dispersion relation and eigenmodes*

To analyse (2.4) with WKB theory, we seek a purely time periodic solution using the so-called physical optics approximation,

$$\boldsymbol{p} \approx \boldsymbol{q}_0(\Phi, \Theta)\, \mathrm{e}^{i(\Sigma(\Phi,\Theta)/\varepsilon - \omega t)}, \tag{3.1}$$

where Σ/ε is a rapidly varying phase function, and $\boldsymbol{q}_0$ a vertical modal structure function of the slow variables $(\Phi, \Theta) = \varepsilon(\phi, \theta)$, where ε is the assumed small WKB parameter, i.e. the ratio of the wavelength of the studied wave to the spatial scale of the topography. As usual, we define a local wavevector $\boldsymbol{k} = \varepsilon^{-1}(\partial_\Phi \Sigma, \partial_\Theta \Sigma)^T$. Inserting (3.1) into (2.4) yields at leading order:

$$(k_\phi \boldsymbol{D}_\phi^\star + k_\theta \boldsymbol{D}_\theta^\star - \omega \boldsymbol{S}) q_0 = 0. \tag{3.2}$$

Equation (3.2) is a generalized (singular) eigenvalue problem which admits two non-trivial solutions. The first is associated with the solvability condition $\det(k_\phi \boldsymbol{D}_\phi^\star + k_\theta \boldsymbol{D}_\theta^\star - \omega \boldsymbol{S}) = 0$, which yields the following dispersion relation:

$$\omega = \frac{(\boldsymbol{\mathcal{U}}_1^\star \cdot \boldsymbol{k})(\boldsymbol{\mathcal{U}}_2^\star \cdot \boldsymbol{k})}{(\boldsymbol{\mathcal{U}}_1^\star + \boldsymbol{\mathcal{U}}_2^\star) \cdot \boldsymbol{k}} = \varpi(\boldsymbol{k}; \phi, \theta), \tag{3.3}$$

or explicitly in terms of the parameters of the problem,

$$\varpi(\boldsymbol{k}; \phi, \theta) = -\frac{g' H_1 k_\phi}{2\Omega R^2 \sin^2\theta} \frac{H_2 + \mu}{H + \mu}, \tag{3.4}$$

where

$$\mu = \tan\theta H'(\phi)\frac{k_\theta}{k_\phi}. \tag{3.5}$$

The regular eigenmode $\boldsymbol{v} = (n_1, n_2)^T$ associated with (3.3) has components satisfying $\mathscr{U}_1^\star \cdot \boldsymbol{k} n_1 + \mathscr{U}_2^\star \cdot \boldsymbol{k} n_2 = 0$. If the normalization condition $\boldsymbol{v}^T \boldsymbol{S} \boldsymbol{v} = 1$ is imposed, which simply means that $|n_1 - n_2| = 1$, we show that

$$n_1(\boldsymbol{k};\phi,\theta) = -\frac{\mathscr{U}_2^\star \cdot \boldsymbol{k}}{(\mathscr{U}_1^\star + \mathscr{U}_2^\star)\cdot \boldsymbol{k}} = -\frac{H_2 + \mu}{H + \mu}, \tag{3.6}$$

$$n_2(\boldsymbol{k};\phi,\theta) = \frac{\mathscr{U}_1^\star \cdot \boldsymbol{k}}{(\mathscr{U}_1^\star + \mathscr{U}_2^\star)\cdot \boldsymbol{k}} = \frac{H_1}{H + \mu}, \tag{3.7}$$

The other non-trivial solution of (3.2) belongs to the null-space of $\boldsymbol{S}$ and is thus proportional to $\mathscr{W} = (1,1)^T$, provided that $\boldsymbol{k}$ satisfies the compatibility condition:

$$(\mathscr{U}_1 + \mathscr{U}_2)\cdot \boldsymbol{k} = 0 \Leftrightarrow \mathrm{J}\left(\Sigma, \frac{H}{f}\right) = 0, \tag{3.8}$$

which is the dispersion relation for this mode, where J(.,.) is the standard Jacobian operator. It is degenerate because it does not involve ω at all, and it is obtained in the limit of vanishing ϵ in the original system (i.e. before making the rigid-lid approximation). In the following, this degenerate solution plays no role and is thus ignored from now on. As for the solution of (3.2), we chose it proportional to $\boldsymbol{v}$; thus, we pose $\boldsymbol{q}_0 = A\boldsymbol{v}$. The determination of A is linked to the so-called transport equation and will be addressed later in the text.

3.2. *Remarks about the number of dynamical modes*

The number of dynamical modes in a layered model is determined by the number of layers. The present system has two layers and thus possesses two dynamical modes. This is not immediately apparent here because the degeneracy introduced by the rigid-lid approximation yields only one dispersion relation of the form $\omega = \varpi(\boldsymbol{k};\phi,\theta)$, giving the impression that the system supports only one mode. The problem occurs because in the limit of vanishing ϵ, the dispersion relation for the flat-bottom barotropic mode behaves like $\omega \sim k_\phi/\epsilon \to \infty$, which is ill-behaved. It follows that although the mode still exists physically, it can no longer be written down explicitly. All is well, however, if the dispersion relation is rewritten in terms of k_ϕ, because then $k_\phi \sim \epsilon\omega$ remains finite. This points to the correct way to retain the two modes explicitly: simply use k_ϕ instead of ω as the eigenvalue of (3.2). This is achieved by rewriting (3.2) as follows:

$$(\omega \boldsymbol{S} - k_\theta \boldsymbol{D}_\theta^\star)\mathscr{V}^\pm = k_\phi^\pm \boldsymbol{D}_\phi^\star \mathscr{V}^\pm, \tag{3.9}$$

with $(k_\phi^+, \mathscr{V}^+)$ and $(k_\phi^-, \mathscr{V}^-)$ the two eigensolutions. Equation (3.9) is a generalized eigenvalue problem which is regular because $\boldsymbol{D}_\phi^*$ – unlike $\boldsymbol{S}$ – is definite positive, hence regular. Note that over a flat-bottom, one root is zero, yielding an infinite phase speed, as noted above, which is the consequence of the rigid-lid approximation. The two eigenvalues k_ϕ^+ and k_ϕ^- are the roots of the following second-order polynomial in k_ϕ:

$$k_\phi^2 + \left(\frac{\mathscr{U}_2^{\star\theta} k_\theta}{\mathscr{U}_2^{\star\phi}} - \frac{\omega \mathscr{U}^{\star\phi}}{\mathscr{U}_1^{\star\phi}\mathscr{U}_2^{\star\phi}}\right) k_\phi - \frac{\omega \mathscr{U}^{\star\theta} k_\theta}{\mathscr{U}_1^{\star\phi}\mathscr{U}_2^{\star\phi}} = 0, \tag{3.10}$$

where $\mathscr{U}^\star = \mathscr{U}_1^\star + \mathscr{U}_2^\star$. Equation (3.10) can also be obtained directly from (3.3);

formally, this yields the two desired dispersion relations under the form $k_\phi = k_\phi^{\pm}(\omega, k_\theta; \phi, \theta)$. The two eigenmodes $\mathscr{V}^+$ and $\mathscr{V}^-$ satisfy the orthogonality condition $\mathscr{V}^{-T}\boldsymbol{D}_\phi^\star\mathscr{V}^+ = 0$, owing to all matrices being symmetric. The components of the two eigenmodes can be obtained by successively inserting k_ϕ^+ and k_ϕ^- into (3.6) and (3.7); as a result, we obtain

$$\mathscr{V}^+ = \mathscr{V}(k_\phi^+) = \begin{pmatrix} -\dfrac{H_2+\mu}{H+\mu} \\ \dfrac{H_1}{H+\mu} \end{pmatrix}, \quad \mathscr{V}^- = \mathscr{V}(k_\phi^-) = \begin{pmatrix} \dfrac{H_2}{\mu} \\ \dfrac{H_2+\mu}{\mu} \end{pmatrix}. \tag{3.11}$$

The flat-bottom case is obtained in the limit $\mu \to 0$, in which case,

$$\mathscr{V}^+ \to \frac{1}{H}\begin{pmatrix} -H_2 \\ H_1 \end{pmatrix}, \quad \mathscr{V}^- \to \frac{1}{\mu}\begin{pmatrix} 1 \\ 1 \end{pmatrix}.$$

These are recognized as the standard flat-bottom baroclinic and barotropic modes, respectively. This shows that using k_ϕ as the eigenvalue of (3.2) instead of ω yields the expected modes over a flat bottom. Another limit of interest is that achieved for $\mu \gg H$, which corresponds to the steep topographic case encountered over the ridge's flanks;

$$\mathscr{V}^+ \to \frac{1}{\mu}\begin{pmatrix} 1 \\ 0 \end{pmatrix}, \quad \mathscr{V}^- \to \frac{1}{\mu}\begin{pmatrix} 0 \\ 1 \end{pmatrix}.$$

These are recognized as the surface and bottom trapped modes, respectively. Finally, note that the properties of these two modes can be exchanged when μ is such that $|H_2 + \mu| \ll 1$, in which case

$$\mathscr{V}^+ \approx \frac{1}{H_1}\begin{pmatrix} 0 \\ 1 \end{pmatrix}, \quad \mathscr{V}^- \approx -\frac{1}{H_2}\begin{pmatrix} 1 \\ 0 \end{pmatrix}.$$

Abrupt changes from bottom-trapped to top-trapped and conversely occur in the present simulations; the same was also described by Hallberg (1997).

3.3. *Ray equations*

The canonical ray equations are given by the well-known Hamiltonian system:

$$\frac{\mathrm{D}\phi}{\mathrm{D}t} = \frac{\partial\varpi}{\partial k_\phi} = c^\star_{g,\phi}, \quad \frac{\mathrm{D}\theta}{\mathrm{D}t} = \frac{\partial\varpi}{\partial k_\theta} = c^\star_{g,\theta}, \tag{3.12}$$

$$\frac{\mathrm{D}k_\phi}{\mathrm{D}t} = -\frac{\partial\varpi}{\partial\phi}, \quad \frac{\mathrm{D}k_\theta}{\mathrm{D}t} = -\frac{\partial\varpi}{\partial\theta}. \tag{3.13}$$

By differentiating (3.4) successively with respect to k_ϕ, k_θ, ϕ and θ, (3.12) and (3.13) are shown to take the form

$$\frac{\mathrm{D}\phi}{\mathrm{D}t} = c^\star_{g,\phi} = -\frac{g'H_1}{2\Omega R^2\sin^2\theta}\frac{(H_2+\mu)^2 + H_1H_2}{(H+\mu)^2}, \tag{3.14}$$

$$\frac{\mathrm{D}\theta}{\mathrm{D}t} = c^\star_{g,\theta} = -\frac{g'H_1}{2\Omega R^2\sin\theta\cos\theta}\frac{H_1H'(\phi)}{(H+\mu)^2}, \tag{3.15}$$

$$\frac{\mathrm{D}k_\phi}{\mathrm{D}t} = \frac{g'H_1k_\phi}{2\Omega R^2\sin^2\theta}\frac{H_1}{(H+\mu)^2}\left(H' + \tan\theta H''\frac{k_\theta}{k_\phi}\right), \tag{3.16}$$

$$\frac{\mathrm{D}k_\theta}{\mathrm{D}t} = \frac{g'H_1k_\phi}{2\Omega R^2\sin^2\theta}\left[\frac{H_1\mu}{(H+\mu)^2}\left(\tan\theta + \frac{1}{\tan\theta}\right) - \frac{H_2+\mu}{H+\mu}\frac{2}{\tan\theta}\right]. \tag{3.17}$$

For completeness, the ray equations (3.14)–(3.17) must be supplemented with initial conditions. For the eastern wavemaker, these are

$$\phi(t=0)=\phi_E, \quad \theta(t=0)=\xi, \tag{3.18}$$

$$k_\phi(t=0)=-\frac{H_0}{H_1(H_0-H_1)}\frac{2\Omega\omega R^2\sin^2\xi}{g'}, \quad k_\theta(t=0)=0, \tag{3.19}$$

which implicitly assumes Σ to be independent of latitude along the eastern boundary through the last condition. The condition for k_ϕ comes from (3.4) assuming a flat bottom (i.e. $H=H_0$) near the eastern boundary.

The group velocity $\boldsymbol{c}_g^\star=(c^\star_{g,\phi},c^\star_{g,\theta})^T$ is obtained by differentiating (3.3) with respect to k_ϕ and k_θ; this yields

$$\boldsymbol{c}_g^\star=\frac{g'}{R^2\cos\theta}\left[\left(\frac{\boldsymbol{\mathcal{U}}_2\cdot\boldsymbol{k}}{(\boldsymbol{\mathcal{U}}_1+\boldsymbol{\mathcal{U}}_2)\cdot\boldsymbol{k}}\right)^2\boldsymbol{\mathcal{U}}_1+\left(\frac{\boldsymbol{\mathcal{U}}_1\cdot\boldsymbol{k}}{(\boldsymbol{\mathcal{U}}_1+\boldsymbol{\mathcal{U}}_2)\cdot\boldsymbol{k}}\right)^2\boldsymbol{\mathcal{U}}_2\right]=n_1^2\boldsymbol{\mathcal{U}}_1^\star+n_2^2\boldsymbol{\mathcal{U}}_2^\star. \tag{3.20}$$

For later use, it is useful to define the two related quantities $\boldsymbol{c}_g=n_1^2\boldsymbol{\mathcal{U}}_1+n_2^2\boldsymbol{\mathcal{U}}_2$, and $\boldsymbol{\gamma}_g=\boldsymbol{\mathcal{C}}\boldsymbol{c}_g$, where $\boldsymbol{\mathcal{C}}$ is the transformation matrix (2.11).

3.4. *Simplification of the ray equations*

The rather complicated canonical ray equations (3.14) to (3.17) can be simplified owing to the fact that the only pieces of information needed to integrate them are: (i) the position, and (ii) the value of the quantity $Z=\tan\theta k_\theta/k_\phi$, as shown for the continuously stratified case over a general topography in Tailleux (2002*a*). Indeed, knowing Z yields $\mu=ZH'(\phi)$ (since H is known everywhere as a function of position), which in turn yields k_ϕ (using 3.4) and then k_θ from the following expressions:

$$k_\phi=-\frac{2\Omega\omega R^2}{g'H_1}\frac{H+\mu}{H_2+\mu}\sin^2\theta, \tag{3.21}$$

$$k_\theta=\frac{Zk_\phi}{\tan\theta}=-\frac{2\Omega\omega R^2}{g'H_1}\frac{Z(H+\mu)}{H_2+\mu}\sin\theta\cos\theta. \tag{3.22}$$

To further simplify the problem, we also use ϕ as the pseudo-time coordinate to describe the ray evolution. This is possible here because $c_{g,\phi}<0$ everywhere, for this makes ϕ a one-to-one function of t. To describe the ray position, we thus only need an evolution equation for θ in terms of ϕ, which is obtained by dividing (3.15) by $c_{g,\phi}$, yielding

$$\frac{\mathrm{d}\theta}{\mathrm{d}\phi}=\frac{\mathrm{D}\theta}{\mathrm{D}t}\Big/\frac{\mathrm{D}\phi}{\mathrm{D}t}=\frac{H_1H'\tan\theta}{(H_2+ZH')^2+H_1H_2}. \tag{3.23}$$

This equation admits the following first integral:

$$\sin\theta=\sin\xi\underbrace{\exp\left\{\int_{\phi_E}^{\phi}\frac{H_1H'}{(H_2+H'Z)^2+H_1H_2}\,\mathrm{d}\phi'\right\}}_{\chi(\phi,\xi)}, \tag{3.24}$$

which yields the following analytical formula for θ:

$$\theta(\phi,\xi)=\arcsin\left(\chi(\phi,\xi)\sin\xi\right), \tag{3.25}$$

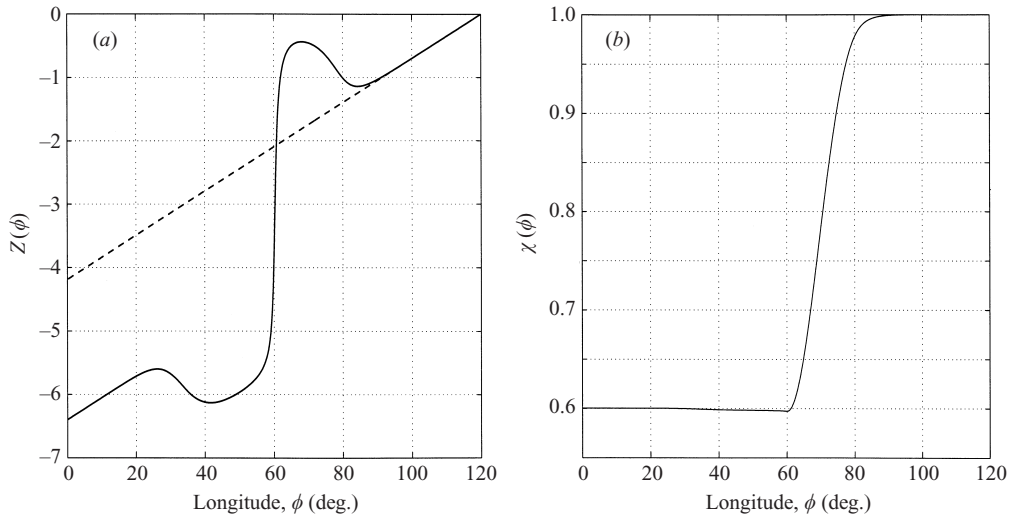

FIGURE 3. (*a*) ——, the function $Z(\phi)$ for the eastern wavemaker experiment corresponding to figure 1, along with $\cdots$, the solution for a flat bottom (dashed line) which is given by $Z = 2(\phi - \phi_E)$, and is thus simply proportional to the distance from the eastern boundary. (*b*) The corresponding function $\chi(\phi)$.

which will prove convenient in the following. To derive an equation for Z, we note that

$$\frac{1}{Z}\frac{\mathrm{d}Z}{\mathrm{d}\phi} = \left(\tan\theta + \frac{1}{\tan\theta}\right)\frac{\mathrm{d}\theta}{\mathrm{d}\phi} + \frac{1}{k_\theta}\frac{\mathrm{d}k_\theta}{\mathrm{d}\phi} - \frac{1}{k_\phi}\frac{\mathrm{d}k_\phi}{\mathrm{d}\phi}. \tag{3.26}$$

Using (3.23) in combination with (3.16) and (3.17) divided by $c_{g,\phi}$, (3.26) becomes

$$\frac{\mathrm{d}Z}{\mathrm{d}\phi} = 2 + \frac{H_1 Z(3H' + H''Z)}{(H_2 + H'Z)^2 + H_1 H_2}. \tag{3.27}$$

By construction, the function χ as defined in (3.24) is always strictly positive. In general, it will depend on both ϕ and ξ. We see, however, that χ can be made independent of ξ provided that ϕ_E and Z are themselves independent of ξ. We verify that this is the case for the wavemaker experiment considered in this study, because (i) the eastern boundary is a meridian, (ii) ξ does not enter (3.27) explicitly, and $Z(\phi_E, \xi) = 0$ from (3.19) is independent of ξ. The functions $Z(\phi)$ and $\chi(\phi)$ corresponding to the experiment depicted in figure 1 are illustrated in figure 3.

3.5. *Consequences for the existence of caustics*

Since the phenomenon of mode conversion is intrinsically a case of WKB breakdown, it seems important to eliminate concern for the possible occurrence of caustics to ascertain that the effects discussed in this paper are unrelated to caustics. By definition, a caustic occurs when two neighbouring rays $\theta(\phi, \xi)$ and $\theta(\phi, \xi + d\xi)$ meet at the same longitude, say ϕ_c. This condition implies

$$\theta(\phi_c, \xi + \mathrm{d}\xi) = \theta(\phi_c, \xi) \Longrightarrow \frac{\partial\theta}{\partial\xi}(\phi_c, \xi) = 0. \tag{3.28}$$

This condition is identical to that derived by KB99 (cf. KB99, equation A.15), but simpler in form here owing to the use of the (ϕ, ξ) coordinates. By differentiating

(3.24) with respect to ξ, the condition (3.28) becomes

$$\frac{\partial\theta}{\partial\xi} = \frac{\cos\xi}{\cos\theta}\chi(\phi_c,\xi) + \frac{\sin\xi}{\cos\theta}\frac{\partial\chi}{\partial\xi}(\phi_c,\xi) = 0. \tag{3.29}$$

Given that χ is always strictly positive, as well as $\sin\xi$ in the northern hemisphere, caustics can only exist if $\partial_\xi\chi < 0$. If χ depends on longitude only, as in the present case, $\partial_\xi\chi = 0$, so that caustics cannot exist here because (3.29) cannot be satisfied. Therefore, some necessary (but not necessarily sufficient) conditions for caustics are that (i) the eastern boundary condition for Z depends on ξ, and (ii) the topography is fully two-dimensional. These results can be shown to extend to the continuously stratified case (Tailleux 2002*a*).

3.6. *Transport equation* (*wave action conservation*)

The simplest way to obtain an amplitude equation for A is directly from the energy conservation (2.13), or more exactly from (2.16) since we are dealing with purely time-periodic solutions. Thus, inserting $\hat{p}_1 = An_1$ and $\hat{p}_2 = An_2$ into (2.16) yields

$$\mathrm{div}(\tfrac{1}{2}\boldsymbol{\gamma}_g A^2) = 0, \tag{3.30}$$

using the result that $\frac{1}{2}[n_1^2\mathscr{C}\mathscr{U}_1 + n_2^2\mathscr{C}\mathscr{U}_2]A^2 = \frac{1}{2}\boldsymbol{\gamma}_g A^2$ from (3.20). This is the standard 'ray tube' conservation of action from Lighthill (1978), where $\boldsymbol{\gamma}_g = \mathscr{C}\boldsymbol{c}_g$ was introduced at the same time as (3.20), thus showing that $\boldsymbol{\gamma}_g$, not $\boldsymbol{c}_g$, is the form of group velocity to be used to recover the usual Cartesian form of ray tube conservation of wave action. As shown in the Appendix, or by direct integration over an infinitesimal surface element bounded between two rays ξ and $\xi + \mathrm{d}\xi$ and two meridians ϕ and $\phi + \mathrm{d}\phi$, (3.30) can be written concisely in the (ϕ,ξ)-coordinate system as follows:

$$\frac{\partial}{\partial\phi}(\theta_\xi c_{g,\phi} A^2) = 0, \tag{3.31}$$

where $\theta_\xi = \partial\theta/\partial\xi$. Physically, $\theta_\xi \mathrm{d}\xi$ represents the distance between two adjacent rays ξ and $\xi + \mathrm{d}\xi$, i.e. the 'width' of the tube. Equation (3.31) is of the form $\partial J/\partial\phi = 0$, where

$$J = \theta_\xi c_{g,\phi} A^2 \tag{3.32}$$

is the standard 'wave action density flux' used in mode conversion theory.

The form (3.31) is particularly useful because it allows us to obtain an explicit analytical expression for A. By integrating (3.31) between an arbitrary interior point $(\phi,\theta(\phi,\xi))$ and the eastern boundary (ϕ_E,ξ) along a ray $\xi = cst$, we thus obtain

$$A^2(\phi,\xi) = \frac{(H_0 - H_1)(H+\mu)^2\chi(\phi)}{H_0((H_2+\mu)^2 + H_1H_2)}A^2(\phi_E,\xi), \tag{3.33}$$

which expresses A in terms of known quantities of ξ and ϕ, as well as in terms of the eastern boundary condition for A. As a consistency check, we verify that $A^2(\phi,\xi) = A^2(\phi_E,\xi)$ over a flat bottom, as $\chi(\phi) = 1$, and $H' = 0$ in that case. In order to obtain an expression for A in terms of ϕ and θ, rather than in terms of ϕ and ξ, simply replace ξ in (3.33) by $\xi(\phi,\theta) = \arcsin(\sin\theta/\chi(\phi))$ which is deduced from (3.25). The result is

$$A^2(\phi,\theta) = \frac{(H_0 - H_1)(H+\mu)^2\chi(\phi)}{H_0((H_2+\mu)^2 + H_1H_2)}A^2(\phi_E,\arcsin(\sin\theta/\chi(\phi))). \tag{3.34}$$

Since $\hat{\eta}_2 = (\hat{p}_2 - \hat{p}_1)/g'$, using $\hat{p}_1 = An_1$ and $\hat{p}_2 = An_2$ show that $\hat{\eta}_2 = A(n_2 - n_1)/g' =$

A/g' given that $n_2 - n_1 = 1$. It follows that $\sqrt{\hat{\eta}_2\hat{\eta}_2^\star} = |\hat{\eta}_2| = A/g'$, so that (3.34) can be used to draw figure 1(*b*).

4. Predictions of mode conversion theory

4.1. *Coupled and uncoupled ray dynamics*

The eigenvalue problem (3.2) is already in a suitable matrix form allowing for an easy application of the standard results of mode conversion theory (the most relevant recent examples are Vanneste 2001 and Hallberg 2001), namely,

$$(\omega \boldsymbol{S} - k_\phi \boldsymbol{D}_\phi^\star - k_\theta \boldsymbol{D}_\theta^\star)\boldsymbol{q}_0 = \begin{bmatrix} D_{11} & D_{12} \\ D_{21} & D_{22} \end{bmatrix} \begin{bmatrix} An_1 \\ An_2 \end{bmatrix} = 0, \tag{4.1}$$

where $D_{11} = \mathscr{U}_1^\star \cdot \boldsymbol{k} - \omega$, $D_{22} = \mathscr{U}_2^\star \cdot \boldsymbol{k} - \omega$, and $D_{12} = D_{21} = \omega$. In fact, it is also in the canonical form considered by Kaufman & Friedland (1987), for instance, where the off-diagonal coefficients $D_{12} = D_{21} = \omega$ are independent of the wave vector and position. This means that here the frequency ω plays the role of the coupling parameter. The strength of the coupling is therefore stronger for higher frequencies whereas it vanishes for steady solutions. The dispersion coefficients D_{11} and D_{22} are regarded as functions of ϕ, k_ϕ and ξ, with ξ treated as a constant as computations are done along a given ray.

In this representation, the implicit equations $D_{11}(\phi, k_\phi, \xi) = 0$ and $D_{22}(\phi, k_\phi, \xi) = 0$ describe the uncoupled ray dynamics, while $(D_{11}D_{22} - D_{12}D_{21})(\phi, k_\phi, \xi) = 0$, which is the second-order polynomial (3.10) for k_ϕ previously considered, describes the actual coupled wave dynamics. Since $\mathscr{U}_1^\star$ and $\mathscr{U}_2^\star$ are independent of the wave vector, the uncoupled dispersion relations $D_{11} = \mathscr{U}_1^\star \cdot \boldsymbol{k} - \omega = 0$ and $D_{22} = \mathscr{U}_2^\star \cdot \boldsymbol{k} - \omega = 0$ actually describe non-dispersive propagation along the potential vorticity contours H_1/f and H_2/f in the upper and lower layers, respectively. These represent the surface- and bottom-intensified Rossby wave modes described by a number of authors, most recently by H97.

Mode conversion occurs near an intersection point for the uncoupled dispersion curves, as is schematically depicted in figure 4 in the (k_ϕ, ϕ)-space. The evolution for k_ϕ and k_θ for the baroclinic ray is given as a function of ϕ and ξ by (3.21) and (3.22). With the notation of figure 4, we will have, therefore,

$$k_\phi^+(\phi, \xi) = -\frac{2\Omega\omega R^2 \sin^2\xi}{g' H_1} \frac{H + H'Z}{H_2 + H'Z} \chi^2(\phi), \tag{4.2}$$

which is (3.21) rewritten by replacing $\sin\theta$ by $\chi(\phi)\sin\xi$. The other root can be easily determined from (3.10) which gives the sum of the roots as $k_\phi^+ + k_\phi^- = Hk_0/H_2 - \mathscr{K}_\theta$, where

$$k_0 = \frac{H_2}{H} \frac{\omega \mathscr{U}^{\star\phi}}{\mathscr{U}_1^{\star\phi} \mathscr{U}_2^{\star\phi}} = -\frac{2\Omega\omega R^2 \sin^2\theta}{g' H_1}, \quad \mathscr{K}_\theta = \frac{\mathscr{U}_2^{\star\theta} k_\theta}{\mathscr{U}_2^{\star\phi}} = \frac{\tan\theta H' k_\theta}{H_2}. \tag{4.3}$$

This yields

$$k_\phi^-(\phi, \xi) = \frac{2\Omega\omega R^2}{g' H_1} \frac{H'Z}{H_2} \sin^2\theta = \frac{2\Omega\omega R^2 \sin^2\xi}{g' H_1} \frac{H'Z}{H_2} \chi^2(\phi). \tag{4.4}$$

Over a flat bottom H' vanishes, so that the two roots reduce to $k_\phi^+ = Hk_0/H_2 = H_0 k_0/H_2$ and $k_\phi^- = 0$, as expected. An example of coupled and uncoupled ray evolution is depicted in figure 5 for $\xi = 35°$, where the coupled rays are given by (4.2) and (4.4),

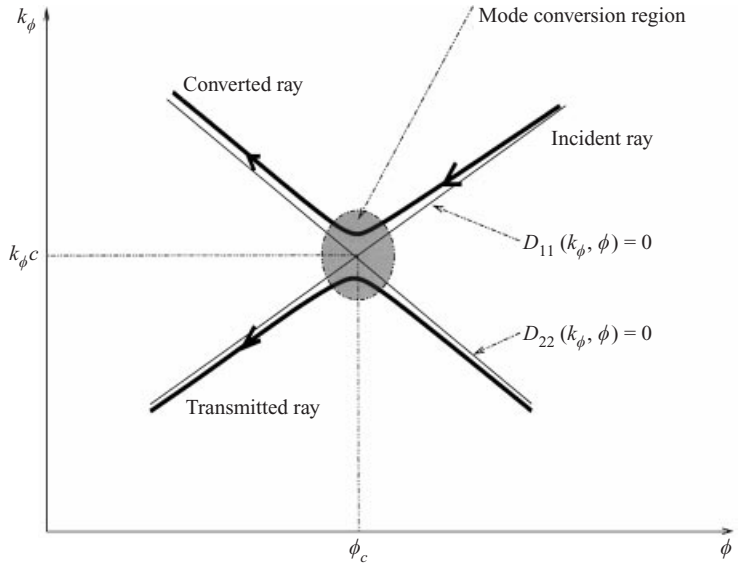

FIGURE 4. Idealized depiction of mode conversion. The two thick lines of equations $k_\phi = k_\phi^+(\phi)$ and $k_\phi = k_\phi^-(\phi)$ represent two branches of the dispersion relation in the (ϕ, k_ϕ)-space. Mode conversion occurs in the shaded area where the incident ray originating from the right-hand side separates into a converted and transmitted ray. The amount of wave action splitting between the two depends on the nature and strength of the mode coupling. The thin lines represent the dispersion curves $D_{11}(k_\phi, \phi) = 0$ and $D_{22}(k_\phi, \phi) = 0$ of the wave modes in the absence of coupling. These curves intersect at the point $(\phi_c, k_{\phi,c})$, where mode conversion is expected to occur for the coupled wave modes.

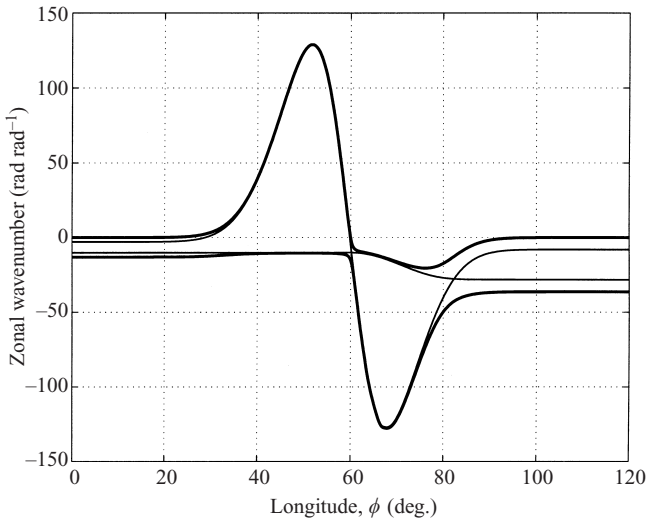

FIGURE 5. Evolution of the ——, coupled and ——, uncoupled wave modes represented in the (k_ϕ, ϕ)-space, as in the previous figure, corresponding to a ray originating at $\xi = 35°N$. The uncoupled rays are the ones intersecting at two locations near the bottom and top of the ridge eastern flank, respectively, where mode conversion must theoretically take place.

and an explicit expression for the uncoupled rays is given in the next section. This figure shows that over the eastern and western flat-bottom parts surrounding the ridge, the uncoupled and coupled wave modes are clearly distinct from each other. This is expected, because the coupled wave modes are the standard flat-bottom baroclinic

and barotropic modes, neither of which are either bottom- or surface-trapped. Over the ridge, however, we see that the uncoupled and coupled wave modes very nearly coincide, clearly evidencing the decoupling effect of the steep topography previously pointed out by a number of authors, e.g. Hallberg (1997).

4.2. *Mode conversion points*

As seen above, the mode conversion points (k_{ϕ_c}, ϕ_c) are located at the intersection of two uncoupled rays; they must therefore simultaneously satisfy $D_{11}(k_{\phi,c}, \phi_c) = D_{22}(k_{\phi,c}, \phi_c) = 0$. To obtain explicit results, it is useful to rewrite D_{11} and D_{22} explicitly as:

$$D_{11}(k_\phi, \phi, \xi) = \mathscr{U}_1^\star \cdot \boldsymbol{k} - \omega = -\frac{g' H_1}{2\Omega R^2 \sin^2 \xi \chi^2(\phi)} [k_\phi - k_1(\phi, \xi)], \tag{4.5}$$

$$D_{22}(k_\phi, \phi, \xi) = \mathscr{U}_2^\star \cdot \boldsymbol{k} - \omega = -\frac{g' H_2}{2\Omega R^2 \sin^2 \xi \chi^2(\phi)} [k_\phi - k_2(\phi, \xi)], \tag{4.6}$$

where the two wavenumbers k_1 and k_2 are given by

$$k_1(\phi, \xi) = -\frac{2\Omega\omega R^2 \sin^2 \xi}{g' H_1} \chi^2(\phi) = k_0(\phi, \xi), \tag{4.7}$$

$$k_2(\phi, \xi) = \left[\frac{H_1}{H_2(\phi)} - \frac{\mu(H + \mu)}{H_2(H_2 + \mu)} \right] k_0(\phi, \xi), \tag{4.8}$$

using the diagnostic expressions (3.21) and (3.22) for k_ϕ and k_θ. With this notation, the two implicit relations $D_{11} = 0$ and $D_{22} = 0$ can be written explicitly as $k_\phi = k_1(\phi, \xi)$ and $k_\phi = k_2(\phi, \xi)$, respectively. The explicit expressions (4.7) and (4.8) are those used to draw the intersecting uncoupled rays of figure 5. The equation for the intersection, therefore, simply becomes $k_1(\phi_c, \xi) = k_2(\phi_c, \xi)$, which provides an equation for ϕ_c, which from (4.7) and (4.8) is given by

$$\mu = -H_2 \pm \sqrt{H_1 H_2}.$$

Only the root with the plus sign yields mode conversion points. This yields

$$H_2(\phi_c) + Z(\phi_c) H'(\phi_c) = \sqrt{H_1 H_2(\phi_c)}. \tag{4.9}$$

Equation (4.9) shows that mode conversion occurs at the same critical longitude(s) for all rays. A graphical solution of (4.9) depicted in figure 6 shows the mode conversion points as the roots of $H_2 - \sqrt{H_1 H_2} + Z H'$. All roots are on the ridge's eastern flank, one near the ridge's bottom and the second near the top, and they coincide with the places where the two uncoupled rays intersect in figure 5.

4.3. *Action splitting at mode conversion points*

In mode conversion theory the converted and transmitted wave action fluxes $J_{converted}$ and $J_{transmitted}$ are linked to the incident wave action flux $J_{incident}$ by the connection formula:

$$J_{transmitted} = T J_{incident}, \tag{4.10}$$

$$J_{converted} = (1 - T) J_{incident}, \tag{4.11}$$

where the transmission coefficient is usually written under the form $T = \mathrm{e}^{-2\pi\nu}$. A general expression for ν is given by equation (4.12) of Flynn & Littlejohn (1994),

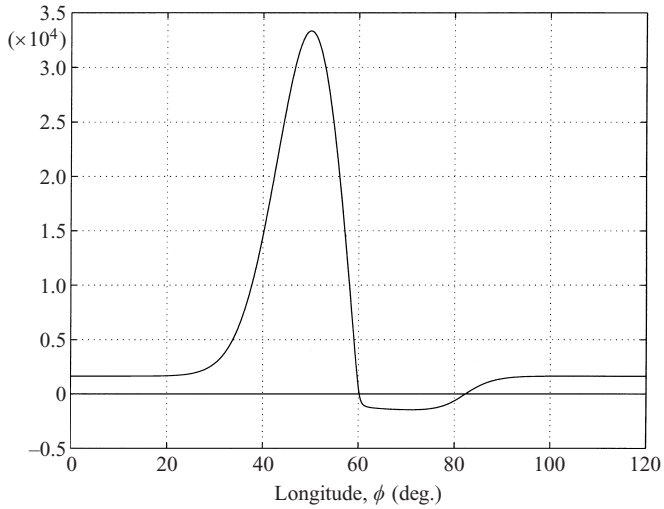

FIGURE 6. The function $H_2(\phi) - \sqrt{H_1 H_2(\phi)} + Z(\phi)H'(\phi) = H_2(\phi) + \mu(\phi) - \sqrt{H_1 H_2(\phi)}$ whose zeros determine the location of the mode conversion points. For this particular example, the coupling points are located at $\phi_1 \approx 60.1864^\circ$ and $\phi_2 = 82.3144^\circ$.

but this reduces to the simpler equation (3) of Kaufman & Friedland (1987) in the present case, namely,

$$v = \left. \frac{\omega^2}{\sqrt{\{D_{11}, D_{22}\}^2}} \right|_{\phi_c, k_{\phi,c}}, \tag{4.12}$$

which involves the Poisson bracket

$$\{D_{11}, D_{22}\} = \partial_\phi D_{11} \partial_{k_\phi} D_{22} - \partial_\phi D_{22} \partial_{k_\phi} D_{11} + \partial_\theta D_{11} \partial_{k_\theta} D_{22} - \partial_{k_\theta} D_{11} \partial_\theta D_{22}. \tag{4.13}$$

(The seemingly different expression used by Hallberg 2001 is the same as (4.12) because $D_{11} = D_{22} = 0$ at the point $(\phi_c, k_{\phi,c})$). To evaluate the Poisson bracket, we must regard D_{11} and D_{22} as functions of all four variables ϕ, k_ϕ, θ and k_θ, i.e. we must use the expressions $D_{11} = \mathscr{U}_1^\star \cdot \boldsymbol{k} - \omega = \mathscr{U}_1^{\star,\phi} k_\phi - \omega$ and $D_{22} = \mathscr{U}_2^\star \cdot \boldsymbol{k} - \omega = \mathscr{U}_2^{\star,\phi} k_\phi + \mathscr{U}_2^{\star,\theta} k_\theta - \omega$; the evaluation of (4.13) is straightforward and yields

$$\{D_{11}, D_{22}\} = \left(\frac{g'}{2\Omega R^2} \right)^2 \frac{H_1}{\sin^2\theta} [3H'(\phi) k_\phi + H''(\phi) \tan\theta k_\theta]. \tag{4.14}$$

This expression is to be evaluated at $k_{\phi,c}$, where

$$k_{\phi,c} = k_1(\phi_c, \xi) = k_2(\phi_c, \xi) = -\frac{2\Omega\omega R^2 \sin^2\theta}{g' H_1}, \tag{4.15}$$

whereas k_θ is evaluated along a ray from (3.22) at $\phi = \phi_c$, yielding

$$k_\theta = -\frac{2\Omega\omega R^2}{g' H_1} \frac{Z(\phi_c)(H(\phi_c) + Z(\phi_c)H'(\phi_c))}{H_2(\phi_c) + H'(\phi_c) Z(\phi_c)} \sin\theta\cos\theta. \tag{4.16}$$

By inserting (4.15) and (4.16) into (4.14), using the result (4.9), the following expression for v is obtained:

$$v = \frac{\Omega\omega R^2 \sin^2\theta}{g' H_1} \left| \frac{2H_1 H'}{(H_2 - H_1)H'' - 3H'^2} \right|_{\phi=\phi_c}. \tag{4.17}$$

An alternative way to write v makes use of Cartesian coordinates by replacing H' by $R\cos\theta H_x$ in (4.17), where $H_x = \mathrm{d}H/\mathrm{d}x$; this yields

$$v = \frac{1}{2}\frac{2\Omega\omega R\sin^2\theta}{g'H_1\cos\theta}\left|\frac{2H_1H_x}{(H_2-H_1)H_{xx}-3H_x^2}\right|. \tag{4.18}$$

In (4.18), we recognize the quantity $c_1 = g'H_1\cos\theta/(2\Omega R\sin^2\theta) = \beta R_1^2$ as the Rossby wave speed of a reduced gravity model, with $R_1 = (g'H_1)^{1/2}/f$ the Rossby radius. Thus, $k_R = \omega/c_1$ is the wavenumber of surface intensified Rossby waves with period ω. Defining

$$L_T = \left|\frac{2H_1H_x}{(H_2-H_1)H_{xx}-3H_x^2}\right|, \tag{4.19}$$

which has the dimension of a length scale, the expression for T becomes

$$T = \exp(-\pi k_R L_T). \tag{4.20}$$

By (4.20), significant transmission occurs only when $k_R L_T \ll 1$. Our expression for v will be compared with equation (2.17) of H01 also derived for a zonally varying topography, but for quasi-geostrophic motions. For easier comparison, we rewrite H01's v in the same form, $v = \frac{1}{2}k_R L_T$, as used in this paper. Using H01's expression (2.7), as well as the condition that $k_1 = k_2$ at mode conversion points (from H01 equation (2.4)), demonstrates that L_T is required to be in the form

$$L_T = \left|\frac{2\omega f H_2}{g'\ell(H_{xx}H_2 - H_x^2)}\right| = \left|\frac{2H_1H_x}{(H_2-H_1)H_{xx}-(H_2-H_1)/H_2H_x^2}\right|, \tag{4.21}$$

where ℓ is H01's notation for the meridional wavenumber. The comparison of (4.19) and (4.21) shows that the two expressions differ only in the term proportional to H_x^2 in the denominator. The two expressions are therefore expected to yield similar results near a mode conversion point where the term proportional to H_{xx} is usually dominant over that involving H_x. Thus, quasi-geostrophy and planetary geostrophy give similar, but not identical, expressions for the transmission coefficient at mode conversion points.

4.4. *Quantitative and qualitative assessment of mode conversion theory*

Figure 7 depicts the square root of the transmission coefficient computed from (4.17) for the two longitudes ϕ_c (e.g. see figure 6) predicted by mode conversion theory. Accordingly, transmission is predicted to be weak at the bottom of the ridge, but significantly more important near the hilltop. Figure 8 shows the numerical simulation reproduced from figure 1(*a*); we superimposed a pair of rays originating from the eastern boundary, starting a new ray each time a mode conversion point was encountered. According to this figure, mode conversion theory is found to be a very good predictor of where to expect wave activity, since the latter is found precisely within the limits delineated by the various rays. To test the theory more quantitatively, we decomposed the numerical solution for $\hat{p}$ on the basis constituted by the two modes $\mathscr{V}^+$ and $\mathscr{V}^-$ as follows:

$$\hat{\boldsymbol{p}} = g'[\hat{\eta}_2^+\mathscr{V}(k_\phi^+) + \hat{\eta}_2^-\mathscr{V}(k_\phi^-)] \tag{4.22}$$

where $\mathscr{V}(k_\phi^+)$ and $\mathscr{V}(k_\phi^-)$ are the two eigenmodes (3.11), while $\hat{\eta}_2^+$ and $\hat{\eta}_2^-$ represent the respective contributions of each mode to the layer interface. From the orthogonality condition for $\mathscr{V}^+$ and $\mathscr{V}^-$, the latter are given by $g'\hat{\eta}_2^\pm = \hat{\boldsymbol{p}}^T D_\phi^\star \mathscr{V}^\pm$. This decomposition is easily achieved in the present case, owing to $\mathscr{V}^+$ and $\mathscr{V}^-$ depending only

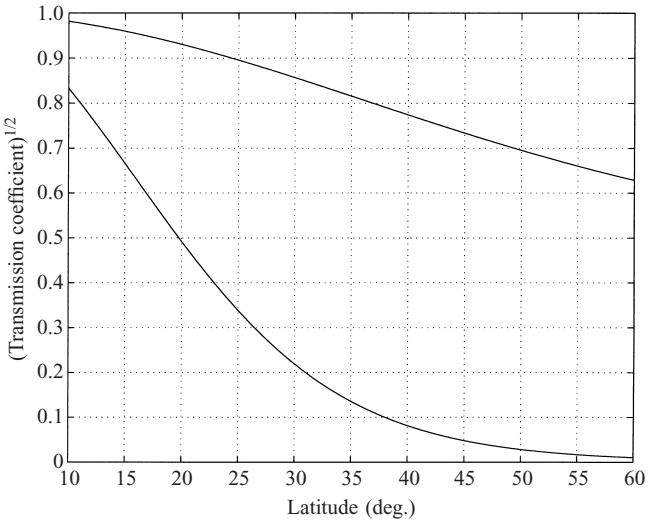

FIGURE 7. Square root of the transmission coefficient as a function of latitude corresponding to the mode conversion point near the ridge's top (upper curve) and that on the eastern flank (lower curve).

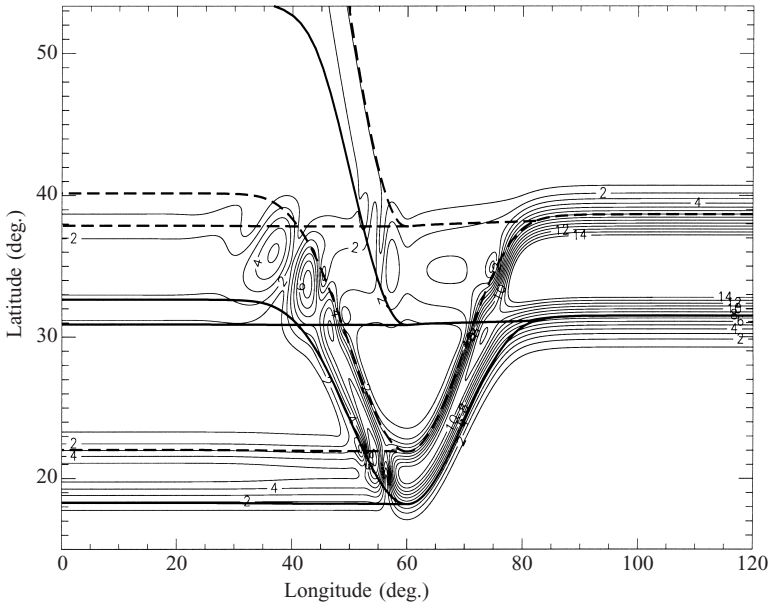

FIGURE 8. A pair of rays (denoted by the heavy solid and dashed lines) originating from the eastern boundary and their successive bifurcations predicted by mode conversion theory superimposed on the direct numerical computation of the r.m.s. interface displacement (reproduced from figure 1*a*).

on ϕ and not on the ray index ξ. Were mode conversion negligible, we would simply have $\hat{\eta}_2^- \approx 0$ and $|g'\hat{\eta}_2^+| = A$. The computed moduli of $|\hat{\eta}_2^+|$ and $|\hat{\eta}_2^-|$ are depicted in figures 9(*b*) and 9(*c*), respectively, whereas figure 9(*a*) shows the prediction of single-mode WKB theory accounting for the two aforementioned mode conversion events. Figure 9(*b*) shows two distinct regions: one originating from the eastern boundary, and one seemingly created near the hilltop. The former is the one expected from

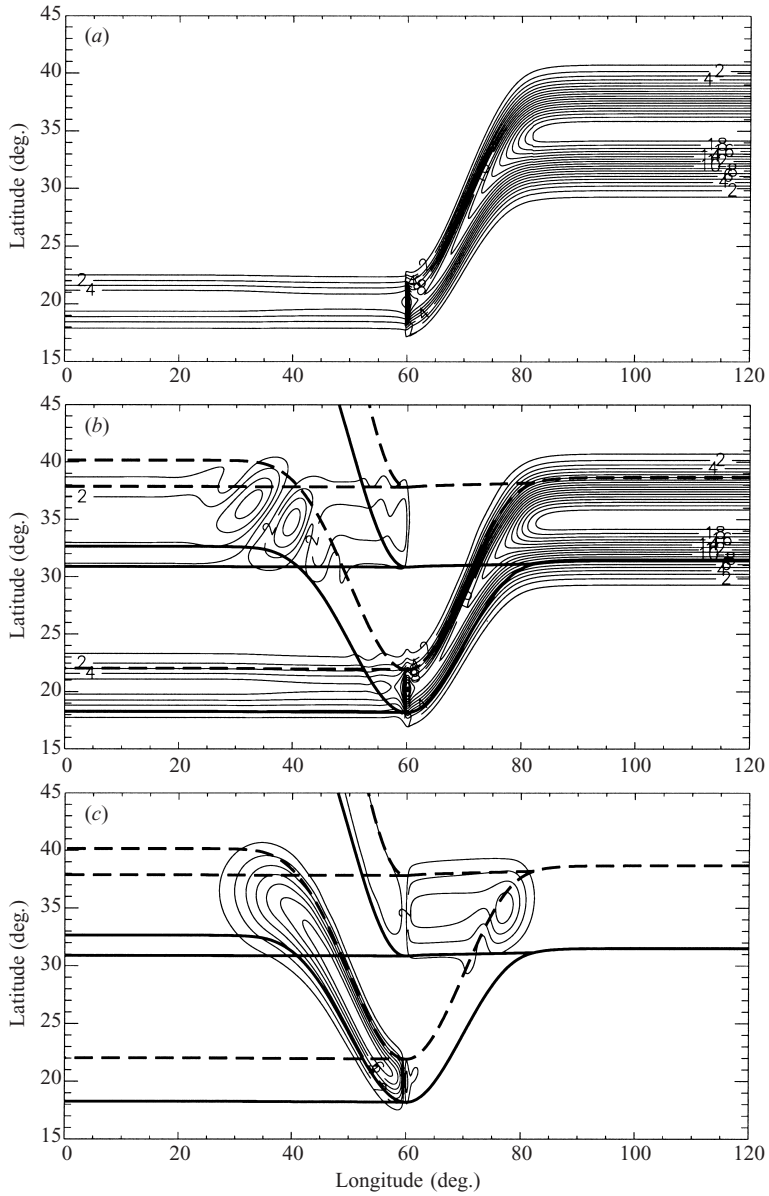

FIGURE 9. (*a*) The root mean square of the layer interface displacement as computed by single WKB mode theory modified to account for the two mode conversion events described in the text. (*b*) The root mean square of the layer interface of the true solution projected on the WKB normal mode. (*c*) The root mean square of the residual of the true layer interface minus the part depicted in (*b*). A pair of rays originating from the eastern boundary and their successive bifurcations predicted by mode conversion theory were superimposed on (*b*) and (*c*).

single-mode WKB theory, and thus the one to be compared with figure 9(*a*). The secondary signal and that depicted in figure 9(*c*), illustrate the importance of mode conversion to explain the numerical simulation, as they would vanish in absence of it. Figures 9(*a*) and 9(*c*) show clearly that mode creation occurs precisely at the predicted mode conversion points where the ray bifurcations occur. Finally, various latitudinal

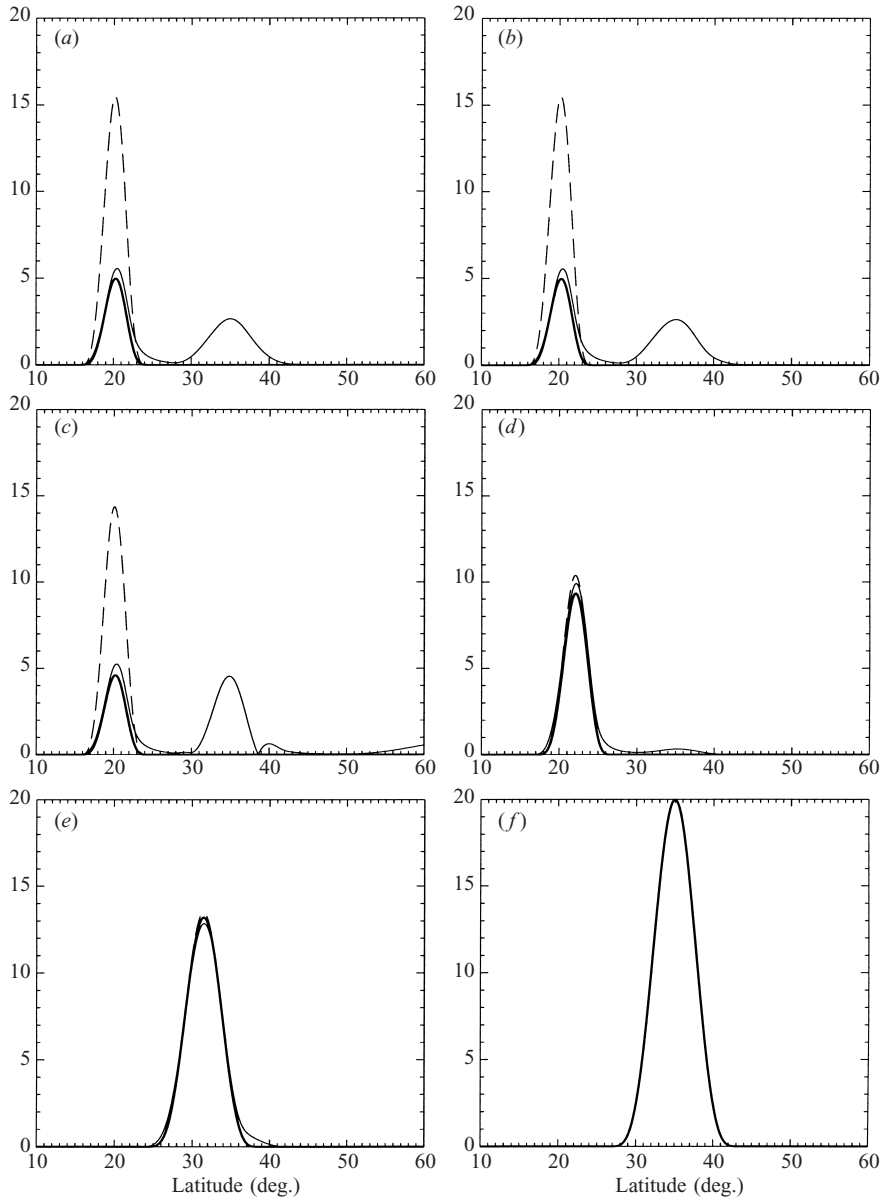

FIGURE 10. Latitudinal sections of $|\hat{\eta}_2|$ computed by: – – –, single WKB mode theory; ——, single WKB mode theory accounting for mode conversion; ——, direct numerical simulation projected on WKB normal mode for various longitudes: (*a*) $\phi = 5°$; (*b*) $\phi = 20°$; (*c*) $\phi = 40°$; (*d*) $\phi = 65°$; (*e*) $\phi = 75°$; (*f*) $\phi = 90°$. In (*d*)–(*f*) the three curves are almost indistinguishable from each other. In (*a*)–(*c*), the additional peak on the right-hand side appears only in the numerical solution, so that the comparison is to be made only for the peak on the left-hand side.

sections of figures 9(*a*) and 9(*b*) are depicted in figure 10 to obtain a more precise idea of the accuracy of mode conversion theory. For comparison, we also added the corresponding sections of the single WKB mode solution of figure 1(*b*). East of the ridge's top (figures 10*d*–10*f*) there is little difference between the true solution and the predictions of single WKB mode theory, with or without accounting for mode

conversion, because transmission remains small. The situation is somewhat different westward of the ridge's top (figures 10*a*–10*c*); there is now a large discrepancy between the true solution and the prediction of single WKB mode theory, as expected, which is considerably reduced by accounting for mode conversion, the remaining error being only a few per cent. Mode conversion appears therefore to be successful both qualitatively and quantitatively.

4.5. *Location of the mode conversion points*

To conclude this section we briefly examine the link between the mode conversion points and the strength of the linear mode coupling. According to (4.20), significant transmission requires low values of L_T. We therefore expect it to occur preferentially near places where L_T is close to zero. To estimate L_T for the Gaussian topography (2.8), we rewrite the expression for H as follows:

$$H(x) = H_0 - \delta H \exp\left\{-\frac{1}{2}\left(\frac{x - x_0}{\ell_T}\right)^2\right\},$$

where $\ell_T = R\cos\theta\delta\phi$, and $x - x_0 = R\cos\theta(\phi - \phi_0)$. From (4.19), we see that L_T is trivially close to zero near a local extremum of H, where $H_x \approx 0$ whereas $H_{xx} \neq 0$. As a result, we expect significant transmission to occur at mode conversion points near the ridge top; but how near should they be? Equation (4.9) shows that linear resonance cannot occur precisely at the top unless $H_2(\phi_c) = H_1$. We disregard this as too particular a case. To treat the general case, we therefore assume $|x_c - x_0|/\ell_T$ small and then expand H as a Taylor series expansion about x_0 in (4.19); this yields the leading-order relation,

$$L_T \approx \frac{2H_1}{|2H_1 + \delta H - H_0|}|x_c - x_0|. \tag{4.23}$$

By combining (4.23) with (4.20) we obtain the following condition on x_c for transmission to be greater than an arbitrarily specified critical value T_{min}:

$$|x_c - x_0| < \frac{2H_1}{|2H_1 + \delta H - H_0|}\frac{|\ln T_{min}|}{\pi k_R}. \tag{4.24}$$

For example, taking $H_0 = 5000$, $\delta H = 1000\,\mathrm{m}$, $H_1 = 1000\,\mathrm{m}$, and $T_{min} = 0.1$ yields $|x_c - x_0| < 0.125\,\lambda_R$, where $\lambda_R = 2\pi/k_R$. Increasing the ridge height to $\delta H = 2000\,\mathrm{m}$ yields $|x_c - x_0| < 0.22\lambda_R$. This suggests that significant transmission is possible only if linear resonance takes place within significantly less than the Rossby wavelength λ_R from the ridge's top. To determine whether x_c falls within this interval, we must solve the implicit equation (4.9) for ϕ_c. Assuming this has been done, expanding (4.9) as a Taylor series around ϕ_c yields the additional condition:

$$|\phi_c - \phi_0| \approx \frac{|H_1 + \sqrt{H_1(H_0 - \delta H - H_1)} + \delta H - H_0|}{\delta H}\frac{\delta\phi^2}{|Z(\phi_c)|}, \tag{4.25}$$

which relates $|x_c - x_0|$ to the parameters of the problem, and to the value of Z at the mode conversion points. This shows that some control of $|\phi_c - \phi_0|$ can be achieved by toying with the values of H_1, δH and H_0, provided that $Z(\phi_c)$ does not vary much while the parameters are modified.

Another less obvious case where L_T can become close to zero is in the asymptotic

limit where $|x - x_0|/\ell_T$ becomes arbitrarily large; indeed, at leading order,

$$L_T \approx \frac{2H_1\ell_T}{|2H_1 - H_0|}\frac{\ell_T}{|x - x_0|}, \quad \frac{|x - x_0|}{\ell_T} \longrightarrow +\infty. \tag{4.26}$$

As in the previous case, this implies a condition on x_c in order for transmission to be greater than the critical value T_{min}, given in this case by

$$\frac{|x_c - x_0|}{\ell_T} > \frac{2H_1}{|2H_1 - H_0|}\frac{\pi k_R \ell_T}{|\ln T_{min}|}. \tag{4.27}$$

Unlike the previous case, significant transmission occurs this time only sufficiently far away from the top of the ridge. It is difficult to say much more, as (4.9) defies a simple analytical treatment in this case.

5. Discussion

In this study, we address the issue of energy propagation for long baroclinic Rossby waves in a two-layer ocean with purely zonal topography within the framework of WKB theory. Of particular interest to us is the problem of mode conversion previously raised by H97, V01 and H01. V01 is ambiguous on whether mode conversion theory is applicable to the particular settings considered by H97, suggesting in particular the possibility of other unspecified non-WKB effects to account for the localized coupling described by H97. H01 is more conclusive in this respect, but does not support its conclusions by the analysis of a specific case. Our study, by comparing a direct numerical simulation to the predictions of WKB and mode conversion theories, definitely establishes the relevance of mode conversion theory. In particular, the possibility that significant transmission may occur is demonstrated. Our study also indicates that WKB theory is a very good descriptor of the 'real' solution, even though the topography considered in this study is quite steep (in the sense that the topographic β effect dominates planetary β, i.e. $fH'(x)/(\beta H) \gg 1$). This is in agreement with H97's conclusions. We speculate that this is due to the particular mathematical structure of the planetary geostrophic equations which often has a quasi-non-dispersive hyperbolic structure. This appears particularly clearly in figure 5 where the uncoupled non-dispersive behaviour is often seen to be very close to the coupled dispersive one. When propagation becomes non-dispersive, WKB theory becomes nearly exact except at mode conversion points which structurally require the solution to be locally expressed in terms of two wave modes.

In this study, our analysis is restricted to only zonal variation of the topography; this is the main cause for the modifications undergone by the zonal wavenumber during westward propagation, which for fixed frequency is responsible for the changes in the zonal phase speed $c_{p,\phi} = \omega/(R\cos\theta k_\phi)$ (seen in measurements by Chelton & Schlax 1996). The main problem in extending the present analysis to a more general topography is the lack of an analytical form for the WKB quantities. However, we do not anticipate meridional variations to affect dramatically our conclusions on mode conversion since these depend essentially on the zonal wavenumber's behaviour. However, meridional topographic variations may yield interesting complications, since they can induce caustics, so that the full two-dimensional case should be studied in detail before definitive conclusions can be drawn (Killworth 2002, personal communication).

A pressing question concerns the extension to a continuously stratified (CS) fluid. In KB99, the scattering of energy between WKB wave modes is neglected, whereas it is shown to be significant in the two-layer simulations of TM00. KB99 argues

plausibly that two-layer models often exaggerate many effects in comparison to their continuously stratified counterpart. As an example, the meridional excursions of the rays are significantly larger in the present two-layer model than in the CS solutions of KB99. Sometimes, however, the opposite occurs. For instance, the speed of surface-intensified first-baroclinic Rossby mode is, in general, underestimated in two-layer model compared to the CS case, as shown in Tailleux & McWilliams (2001). This argument comes back to the qualitative and quantitative differences between a two-layer ocean model and a continuously stratified model, analysed in detail in Flierl (1978). To assess the relevance of mode conversion to the CS case, Tailleux (2002*a*) and Tailleux (2002*b*) numerically computed instances of rays for the same kinds of experiment as presented here, but for a continuous exponential stratification and constant buoyancy frequency, respectively. In both cases, the top of the ridge is found to be associated with very rapid changes taking place within less than 2°, which is much shorter than the wavelengths of interest. For this reason, we are strongly inclined to believe that mode conversion is also relevant to the continuously stratified case. According to Killworth (2002, personal communication), the ridge's top appears to be a region associated with stiff numerics, which make it difficult to conserve the frequency along the rays. All this indicates that the ridge's crest is a place associated with non-standard ray dynamics, which we must now look at more closely.

To make further progress, the details of mode conversion theory for a continuously stratified fluid must be determined. In particular, we must understand how the length scale L_T which enters the definition of the transmission coefficient, is related to the topography and stratification in the general case. Only then will we be able to settle definitely the question of whether mode conversion is relevant to the actual ocean. To address mode conversion in a continuously stratified fluid, the main difficulty probably consists in reducing the problem to the standard form. This requires identifying the 'uncoupled' wave modes and the coupling mechanism. In the two-layer model, the uncoupled wave modes are found to be the layer modes propagating non-dispersively along the H_i/f contours, whereas the coupling parameter is found to be ω. Since there is no obvious equivalent to the layer thicknesses H_i in a continuously stratified fluid, the identification of the relevant quantities in this case is an interesting topic for future study.

The authors would like to thank John Allen and Roger Grimshaw for providing references to their work, as well as Jacques Vanneste and Allan Kaufman for pointing out relevant works in plasma physics and useful comments. We thank Bob Hallberg and Peter Killworth for useful comments and discussions. This work was supported by the National Science Foundation through grant OCE-9633681 and the National Aeronautics and Space Administration through grant NAG5-3982.

Appendix. Action conservation in (ϕ, ξ) coordinates

To demonstrate (3.31), we first establish the following lemma:

LEMMA 1. *Let (F_ϕ, F_θ) be an arbitrary differentiable vector field. Then,*

$$\frac{\partial F_\phi}{\partial \phi} + \frac{\partial F_\theta}{\partial \theta} = \frac{1}{\theta_\xi}\left[\left(\frac{\partial(\theta_\xi F_\phi)}{\partial \phi}\right)_\xi + \left(\frac{\partial}{\partial \xi}\left(F_\theta - \theta_\phi F_\phi\right)\right)_\phi\right]. \tag{A 1}$$

Proof. For an arbitrary scalar field $\mathcal{Q}$, the chain rule yields

$$\left(\frac{\partial \mathcal{Q}}{\partial \phi}\right)_{\xi} = \left(\frac{\partial \mathcal{Q}}{\partial \phi}\right)_{\theta} + \left(\frac{\partial \mathcal{Q}}{\partial \theta}\right)_{\phi} \left(\frac{\partial \theta}{\partial \phi}\right)_{\xi}, \tag{A 2}$$

$$\left(\frac{\partial \mathcal{Q}}{\partial \xi}\right)_{\phi} = \left(\frac{\partial \mathcal{Q}}{\partial \theta}\right)_{\phi} \left(\frac{\partial \theta}{\partial \xi}\right)_{\phi}. \tag{A 3}$$

These relations are inverted as follows:

$$\left(\frac{\partial \mathcal{Q}}{\partial \theta}\right)_{\phi} = \frac{1}{\theta_{\xi}} \left(\frac{\partial \mathcal{Q}}{\partial \xi}\right)_{\phi}, \tag{A 4}$$

$$\left(\frac{\partial \mathcal{Q}}{\partial \phi}\right)_{\theta} = \left(\frac{\partial \mathcal{Q}}{\partial \phi}\right)_{\xi} - \frac{\theta_{\phi}}{\theta_{\xi}} \left(\frac{\partial \mathcal{Q}}{\partial \xi}\right)_{\phi}, \tag{A 5}$$

where for conciseness, we use the notation $(\partial_{\xi}\theta)_{\phi} = \theta_{\xi}$ and $(\partial_{\phi}\theta)_{\xi} = \theta_{\phi}$. (Note that $\theta_{\phi} = c_{g,\theta}/c_{g,\phi}$.) From the passage relations (A 4) and (A 5), it follows that

$$\frac{\partial F_{\phi}}{\partial \phi} + \frac{\partial F_{\theta}}{\partial \theta} = \left(\frac{\partial F_{\phi}}{\partial \phi}\right)_{\xi} - \frac{\theta_{\phi}}{\theta_{\xi}} \left(\frac{\partial F_{\phi}}{\partial \xi}\right)_{\phi} + \frac{1}{\theta_{\xi}} \left(\frac{\partial F_{\theta}}{\partial \xi}\right)_{\phi}. \tag{A 6}$$

Furthermore, we also have

$$\left(\frac{\partial (\theta_{\xi} F_{\phi})}{\partial \phi}\right)_{\xi} = \theta_{\xi} \left(\frac{\partial F_{\phi}}{\partial \phi}\right)_{\xi} + \theta_{\phi\xi} F_{\phi}, \tag{A 7}$$

$$\left(\frac{\partial (\theta_{\phi} F_{\phi})}{\partial \xi}\right)_{\phi} = \theta_{\phi} \left(\frac{\partial F_{\phi}}{\partial \xi}\right)_{\phi} + \theta_{\phi\xi} F_{\phi}. \tag{A 8}$$

By differentiating (A 1), accounting for (A 7) and (A 8), we see that (A 1) and (A 6) are equivalent. This concludes the proof. Now, since $\theta_{\phi} = c_{g,\theta}/c_{g,\phi}$, it follows that $c_{g,\theta}A^2 - \theta_{\phi} c_{g,\phi} A^2 = 0$, so that applying the lemma to (3.30) yields (3.31). □

REFERENCES

Allen, J. S. & Romea, R. D. 1980 On coastal trapped waves at low latitudes in a stratified ocean. *J. Fluid Mech.* **98**, 555–585.

Chelton, D. B. & Schlax, M. G. 1996 Global observations of oceanic Rossby waves. *Science* **272**, 234–238.

Dewar, W. K. 1998 On 'too fast' baroclinic planetary waves in the general circulation. *J. Phys. Oceanogr.* **28**, 1739–1758.

Flierl, G. R. 1978 Models of vertical structure and the calibration of two-layer models. *Dyn. Atmos. Oceans* **2**, 341–381.

Flynn, W. G. & Littlejohn, R. G. 1994 Normal forms for linear mode conversion and Landau–Zener transitions in one dimension. *Ann. Phys.* **234**, 334–403.

Gill, A. E. 1982 *Atmosphere Ocean Dynamics.* Academic.

Grimshaw, R. & Allen, J. S. 1979 Linearly coupled, slowly varying oscillators. *Stud. Appl. Maths* **61**, 55–71.

Hallberg, R. 1997 Localized coupling between surface and bottom-intensified flow over topography. *J. Phys. Oceanogr.* **27**, 977–998.

Hallberg, R. 2001 Reply (to 'Comments on localized coupling between surface and bottom intensified flow over topography'). *J. Phys. Oceanogr.* **31**, 1926–1930.

Holland, W. R. 1967 On the wind-driven circulation in an ocean with bottom topography. *Tellus* **19**, 582–599.

Kaufman, A. N. & Friedland, L. 1987 Phase-space solution of the linear mode conversion problem. *Phys. Lett*. A **123**, 387–389.

Kaufman, A. N., Morehead, J. J., Brizard, A. J. & Tracy, E. R. 1999 Mode conversion in the Gulf of Guinea. *J. Fluid Mech.* **394**, 175–192.

Killworth, P. D. & Blundell, J. R. 1999 The effect of bottom topography on the speed of long extratropical planetary waves. *J. Phys. Oceanogr*. **29**, 2689–2708.

Killworth, P. D., Chelton, D. B. & deSzoeke, R. 1997 The speed of observed and theoretical long extratropical planetary waves. *J. Phys. Oceanogr*. **27**, 1946–1966.

Leblond, P. H. & Mysak, L. A. 1978 *Waves in the Ocean.* Elsevier.

Lighthill, J. 1978 *Waves in Fluids.* Cambridge University Press.

Liu, Z. Y. 1999 Planetary waves in the thermocline: non-Doppler-shift mode, advective mode and Green mode. *Q. J. Roy. Met. Soc*. **125**, 1315–1339.

Sakamoto, T. & Yamagata, T. 1997 Evolution of baroclinic planetary eddies over localized bottom topography in terms of JEBAR. *Geophys. Astrophys. Fluid Dyn.* **84**, 1–27.

Tailleux, R. 2002*a* On the ray dynamics of long baroclinic Rossby waves over topography. *J. Phys. Oceanogr*. (in press).

Tailleux, R. 2002*b* A WKB analysis of the surface signature of long extratropical baroclinic Rossby waves over topography. *Ocean Modelling* (in press).

Tailleux, R. & McWilliams, J. C. 2000 Acceleration, creation, and depletion of wind-driven, baroclinic Rossby waves over an ocean ridge. *J. Phys. Oceanogr*. **30**, 2186–2213.

Tailleux, R. & McWilliams, J. C. 2001 The effect of bottom pressure decoupling on the speed of extratropical, baroclinic Rossby waves. *J. Phys. Oceanogr*. **31**, 1461–1476.

Vanneste, J. 2001 Mode conversion for Rossby waves over topography: Comments on 'Localized coupling between surface and bottom-intensified flow over topography'. *J. Phys. Oceanogr*. **31**, 1922–1925.